Institute for Photogrammetry

Geschwister-Scholl-Str. 24D
D-70174 Stuttgart
Tel.: +49 711 685 83336
Fax: +49 711 685 83297
info@ifp.uni-stuttgart.de
http://www.ifp.uni-stuttgart.de

Head of Institute

Prof. Dr.-Ing. Uwe Sörgel

Deputy:	apl. Prof. Dr.-Ing. Norbert Haala
Personal Assistant:	Martina Kroma
Emeritus Professors:	Prof. Dr.-Ing. Dr. hc. mult. Fritz Ackermann
	Prof. Dr.-Ing. Dieter Fritsch

Academic Staff

Dr.-Ing. Susanne Becker (until 8/2017)	Hybrid GIS
Dipl.-Ing. Alessandro Cefalu	Photogrammetric Calibration
Dr.-Ing. Michael Cramer	Photogrammetric Systems
Dipl.-Ing.(FH) Markus Englich	Laboratory, Computing Facilities
apl. Prof. Dr.-Ing. Norbert Haala	Photogrammetric Computer Vision
MSc. Dominik Laupheimer (since 11/2017)	Classification in Remote Sensing
Dr. techn. Gottfried Mandlburger	Laser Bathymetry
MSc. Lavinia Runcenau	Modelling of Building Interiors
Dipl.-Ing. Patrick Tutzauer	Facade Interpretation
Dr.-Ing. Volker Walter	Geoinformatics
MSc. Chia-Hsiang Yang	Persistant Scatterer Interferometry

Stipendiaries and external PhD Students

MSc. Stefan Cavegn	Image-based Mobile Mapping
MSc. Ke Gong	3D Reconstruction
Dipl.-Ing. Wolfgang Groß	Transformation of Hyperspectral Data
Dipl.-Phys. Hendrik Schilling	Classification of Hyperspectral Data
MSc. Mehrdad Nekouei Sharaki	Photogrammetric Image Processing

Guests

MSc. Mateusz Karpina	Interpretation of 3D point clouds
MSc. Rodolfo Lotte	Image Processing
MSc. Jinghui Wang	Surface Motion Estimation

External Teaching Staff

Dipl.-Ing. Stefan Dvorak, Amt für Stadtentwicklung und Vermessung, Reutlingen

Research Activities in ifp organized in four thematic Groups

Geoinformatics	Dr.-Ing. Volker Walter
Photogrammetric Computer Vision	apl. Prof. Dr.-Ing. Norbert Haala
Photogrammetric Systems	Dr.-Ing. Michael Cramer
Remote Sensing	Prof. Dr.-Ing. Uwe Sörgel

Research Projects

Indoor change detection

A large variety of systems for mapping and interpretation of outdoor environments can process automatically updated 3D models. However, there is still ongoing research on processing similar models for indoor space. A challenging problem in the field of Building Information Modelling (BIM) is to maintain up-to-date models. Even though, not for every building a BIM model is available, for some of them older laser scanner point clouds are available which can be used as a reference for the comparison with a current model.

As a first step in automatic detecting of indoor changes, we used an indoor terrestrial laser scanner (TLS) point cloud composed of 31 individual scans. The available scans were saved in an octree structure. Considering the scanner positions, it was possible to use a ray-tracing algorithm in order to differentiate between three different states. Each octree cell is considered to be occupied if there are points inside. The cell is assigned as free if at least one ray is passing through it, or the state is considered to be unknown. Using this structure, it can be further investigated if the model is corresponding with a previous available model. Also the situation can be studied, when further changes occur and we are aware of them and of their approximate location. In this case, a low cost device with a range sensor (like Google Tango) could be used to monitor the changes. The octree structure will allow an update of the corresponding part of the model, by simply changing the state of the corresponding voxels.

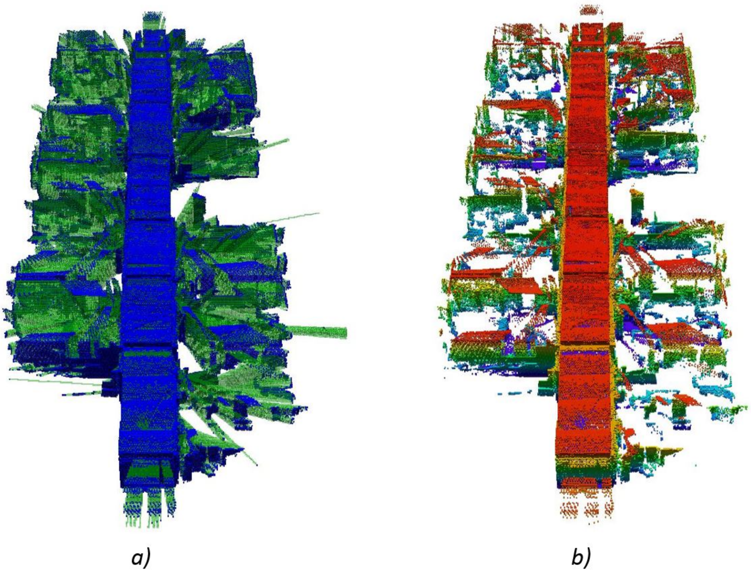

Figure 1: Occupancy map visualized with octovis: a) blue: occupied, green: free, transparent: unknown octree volumes; b) height map (color coded) (A. Hornung, K.M. Wurm, M. Bennewitz, C. Stachniss, and W. Burgard, „OctoMap: An Efficient Probabilistic 3D Mapping Framework Based on Octrees“ in Autonomous Robots, 2013)

Deep Learning based interpretation of publicly available facade imagery and perceptual rules for building enhancements

Enrichment of urban building models with semantics is an active research question in the field of geoinformation and geovisualization. Semantic information is not only valuable for applications like Building Information Modeling (BIM) but also offers possibilities to enhance visual insight for humans when interacting with such data. Presenting users the highest level of detail of building models is often neither the most informative nor feasible way - for instance, when using mobile apps, resources and display sizes are quite limited. A concrete use case is the imparting of building use types in urban scenes to users. In the first part of our work, we first try to determine use types of buildings by means of a Deep Learning approach. Once building categories are determined, the second part of our work focuses on embedding this knowledge into building category-specific grammars to modify automatically the geometry of a building to align its visual appearance to its underlying use type.

Deep Learning based interpretation of publicly available facade imagery

In order to enrich 3D urban models autonomously, we train Convolutional Neural Networks (CNNs) for classifying street-view images of building facades into five different use classes. The classes „commercial" and „residential" represent a singular use of a building, while the class „hybrid" represents a mixture of these two use classes. The class „specialUse" represents the remaining buildings not matching the other three classes, like e.g. schools and churches. Finally, the class „underConstruction" contains buildings being under construction independently on their actual use.

CNNs are a data-driven end-to-end approach. Hence, there is no need for human-crafted features. Instead, the network learns decisive features during the training process. For this learning, a huge amount of labeled data (training set) has to be provided. I.e. for every street-level image of the training set, the ground truth class is known.

In our case, the ground truth data consists of the digital city base map provided by the City Survey Office Stuttgart linked with the respective street level images based on positions and headings as provided by the Street View API.

After training, the network can be applied to any previously unseen image. The network will output a probability density function over the five classes. As it is an end-to-end approach (i.e. a black box), humans cannot understand how CNNs classify the way they do.

With the help of so-called Class Activation Maps (CAMs) learned features can be localized and interpreted within input images. CAMs are heat maps that highlight image sections, which are decisive for the respective labeling. Thereof, a human operator can derive learned features, which are useful for understanding the networks decisions. Figure 2 shows correctly classified images and misclassified images overlaid by the associated CAMs, which highlight decisive image parts.

Another application of CAMs is their use as importance maps for non-photorealistic renderings. This process should maintain a high level of detail for important regions, while less important ones are abstracted. Thus, a CAM-based abstraction using the provided importance maps can help to focus a human viewer's attention to important regions for the visual discrimination of building categories. This abstract rendering is based on stippling, which is frequently used in architecture for sketching and illustration purposes. For matching the tone and texture of an image, visually similar point sets are created: in dark areas, many points are used and, conversely, only few points are used in bright regions. An increasing degree of abstraction is achieved by reducing the amount of points in the less important regions (provided by CAMs) while increasing the point size. In this way, smaller details are removed progressively. Figure 3 depicts a stippled result created without the usage of the corresponding CAM and the focus with a constant point size and no brightening (left) versus results created with our pipeline (right). The area in focus (bright regions in the grayscale CAM in the middle) is clearly distinguishable from the rest in our result.

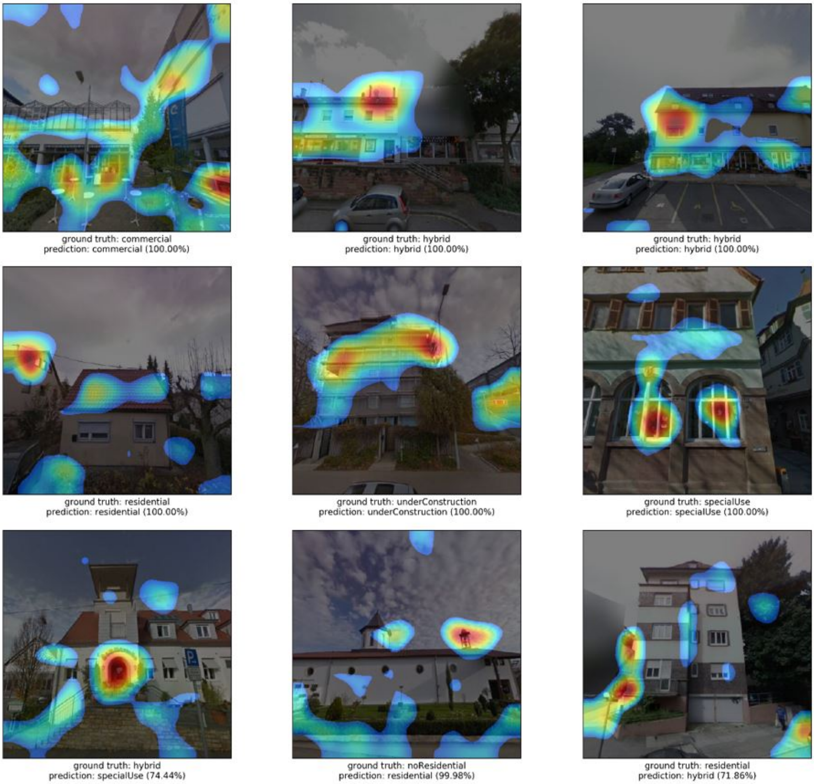

Figure 2: First two rows: Correct classifications of a CNN with overlaid CAMs. Bottom row: Misclassifications.

Figure 3: Created stipple drawings without (left) and with (right) usage of the grayscale CAM (center) to focus the user's attention. Focus in this example is on the door area.

Perceptual rules for building enhancements

Every building has a set of properties that refer to a certain use type. To generate virtual representations of buildings which are easily understandable for humans, we need to refine or abstract (in general - adapt) those buildings in a certain manner. Thus, specific rule sets were designed for each building category. These rule sets incorporate geometric and semantic constraints we extracted from our previous user studies by relating the features of ground truth buildings with as-perceived classifications by users - as an example - add balconies to a Residential Tower if they are not existent. We use those rules either to generate use-type specific buildings from scratch or to adapt existing ones. For the latter it is important to maintain the key characteristics of a building - therefore, we feed essential building elements of a previously parsed CityGML model into the modelling process. Figure 4 shows the application of building category-specific rules to a coarse building model. If a building category is not known beforehand or not inferable the way discussed in the previous section, we can use the parsed CityGML model to derive essential building features (such as building footprint, number of floors, floor height, ...). Mapping the model into building feature space and performing a nearest neighbor search returns the most probable building category. The class centers in feature space are mean buildings for each category that we computed based on data from previous user tests.

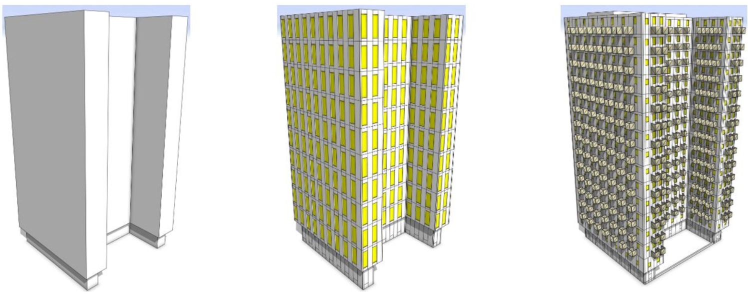

Figure 4: From left to right: Coarse model of a building tower; enhanced building with generic Office Building rules; enhanced building with generic Residential Tower rules.

Robust and accurate image-based georeferencing exploiting relative orientation constraints

Image-based mobile mapping systems featuring multi-view stereo camera configurations enable efficient data acquisition, for both outdoor and indoor environments. In order to obtain accurate geospatial 3D image spaces consisting of collections of georeferenced multi-view RGB-D imagery, which can be exploited for 3D mono-plotting applications as well as for 3D point cloud and mesh generation, depth maps of high quality need to be computed. These depth maps are preferably generated by performing multi-view stereo matching using imagery captured at different epochs. In order to efficiently apply coplanarity constraints during dense stereo matching, sub-pixel accurate relative orientations of the image sequences are required. Since we rely on revealed trajectory discontinuities from direct georeferencing of up to 15 cm in urban environments, this can only be achieved by image-based georeferencing. This allows the elimination of trajectory offsets in the range of several decimeters leading to consistent image sequences, which might be captured at different days and daytimes.

In order to perform an integrated georeferencing, we extended the powerful incremental structure-from-motion (SfM) tool COLMAP, thus assuming initial values for exterior orientation parameters (EOP) from direct sensor orientation or SLAM (see Figure 5). First, we extract SIFT features in outdoor and DSP-SIFT in indoor environments with poor texture. Since we rely on prior EOP, we use the spatial feature matcher implemented in COLMAP, which only considers camera positions closer than a given maximum radius from the current image for search space reduction. Moreover, we added a maximum angle constraint in order to further speed up the process as feature matching is the most time consuming step in the COLMAP procedure. Feature extraction and matching is followed by geometric verification, resulting in a scene graph that serves as the foundation for the reconstruction stage.

Second, we triangulate 2D image features to natural 3D points incorporating all available images based on prior EOP, followed by bundle adjustment using Google's Ceres Solver library. Our bundle adjustment procedure not only minimizes the reprojection errors between the projected natural 3D points as well as ground control points (GCP) and its corresponding 2D measurements in image space, but it also minimizes differences of 3D projection center coordinates from direct georeferencing and photogrammetric reconstruction. Moreover, we constrain calibrated relative orientation parameters (ROP) or define constraints for ROP among cameras in bundle adjustment. Subsequently, COLMAP completes 3D point tracks, merges 3D points that are very close to each other, filters and re-triangulates observations before performing a new bundle adjustment computation. This iterative process is continued until convergence is reached.

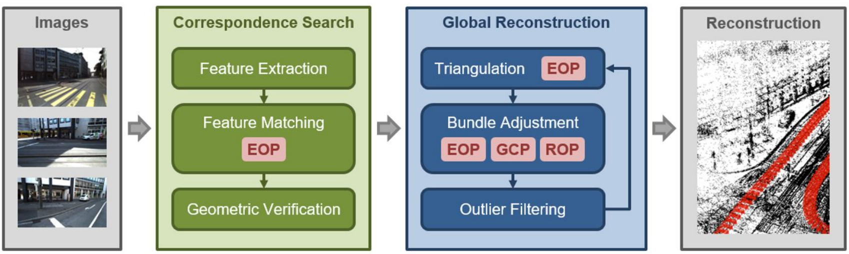

Figure 5: Adapted processing pipeline of COLMAP based on prior exterior orientation parameters and a limited number of ground control points as well as exploiting constraints for relative orientation parameters among all cameras.

We evaluated our integrated georeferencing approach on two data sets, one captured outdoors in Basel by a vehicle-based multi-stereo mobile mapping system and the other captured indoors in Muttenz close to Basel by a portable panoramic mobile mapping system (see Figure 6). We obtained mean RMSE values for check point residuals between image-based georeferencing and tachymetry of 2 cm in an indoor area, and 3 cm in an urban environment where the measurement distances are a multiple compared to indoors. Moreover, in comparison to a solely image-based procedure, our integrated georeferencing approach showed a consistent accuracy increase by a factor of 2-3 at our outdoor test site. Due to pre-calibrated relative orientation parameters, images of all camera heads were oriented correctly in our indoor environment, even though they hardly overlap as well as they mainly contain homogenous surfaces or repetitive patterns. By performing self-calibration of relative orientation parameters among respective cameras of our vehicle-based mobile mapping system, remaining inaccuracies from suboptimal test field calibration were successfully compensated.

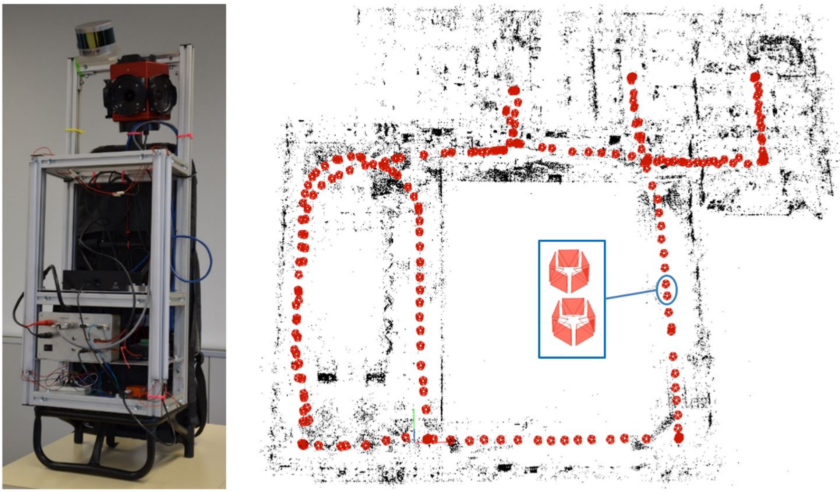

Figure 6: Sensor configuration of the portable mobile mapping system of the Institute of Geomatics (IGEO), University of Applied Sciences and Arts Northwestern Switzerland (FHNW) (left) as well as georeferenced mobile mapping images (red) and 3D tie points (black) at our indoor test site using our modified COLMAP processing pipeline (right).

On the potential of low-cost UAV camera systems

In former photogrammetry much effort was spent into the development of highly precise and stable camera systems, which are known since decades. Similar concepts have also been applied, when analog imaging moved into digital. With the advent of unmanned aircraft vehicles (UAV) this concept changed, mostly due to the limited maximum take-off-mass

(MTOM) of those systems. Typically an MTOM within 10kg should not be exceeded. This in a way prevents the use of stable, but also heavier and bulkier systems. This is, why regular consumer grade cameras are used quite often. Alternatively, manufactures combine their UAV-platform with proprietary cameras, which are often optimized for taking video sequences. Still, such commercial and quite low-cost UAVs increasingly are used for photogrammetric surveys. As an example the dji products of the Phantom or Inspire series could be mentioned, which have been established to map 3D structures of limited size. The wide distribution of such platforms is due to their easy use and attractive price. Many users, like engineering offices, who now have extended their terrestrial survey portfolio by UAV-based mapping, have invested in dji UAVs. As the classical photogrammetry has its clear focus on the precise geometric modelling of 3D objects, the geometric calibration and stability is one important part of the process flow. From this point of view, almost all UAV camera systems belong to the group of „partially metric cameras“ since the sensor matrix realizes a defined image coordinate system and the distortion parameters of the interior orientation can be assumed to be largely constant, while focal length and principal point position represent variable elements. From this, the necessity for camera calibration is obvious, which most often is carried out simultaneously within the bundle block adjustment of project data itself - this is called self- / or in-situ calibration, allowing the optimal estimation of camera calibration as part of the project itself. In order to analyze the potential of low cost UAV cameras, extensive tests have been made to estimate their geometric stability and performance. In order to have reproducible results most of these tests have been made in controlled laboratory environments. Figure 7 shows the 3D test field for geometrically camera calibration in the photogrammetric lab at the Institute for Photogrammetry (ifp). Such test site allows for the precise estimation of geometric camera calibration parameters. If such (geometric) calibrations is done several time, where the individual calibration runs are spread over a longer period of time, the geometrical stability of the camera system can also be evaluated. As it can be seen from Figure 7, additional Siemens star targets are distributed in addition to the coded targets. Such resolution targets are used to derive the true physical resolution of the sensor, which serves as an additional quality parameter of the camera system.

Figure 8 now depicts the change of the principal point coordinates of different camera models. The three dji systems Phantom 4, Phantom 4pro, MAVIC are compared against the Nikon D800 DSLR with 35mm lens as the reference system. As you can see, the results from multiple calibration runs are illustrated. These tests have been made on several days, sometimes the systems additionally have been warmed up or cooled down to simulate different environmental conditions. In addition the calibrations have been done using the original camera raw images (converted to TIF) and the JPG images, as provided by the camera directly. Every graph shows a 4 x 6 pixel wide area, except for the MAVIC system. Here the variations in the principal point are much larger. Thus a 12 x 9 pixel wide area is depicted here.

It is surprising to see, that the Phantom 4 camera shows the smallest variations within the different calibration runs. Except one measurement, where the principal point coordinates are little more far away, all other results are within one large cluster, which clearly indicates a quite stable camera configuration. The reason for this is the stable concept of the Phantom 4

Figure 7: 3D test site for geometrical camera calibration in the ifp measurement lab. In addition to the coded target, several Siemens stars are distributed in the test field to estimate the physical resolution of the sensor system.

camera, with fix mounted and focused lens, which is close to the classic concept of metric cameras. Then the D800 shows the most stable behavior followed by the Phantom 4pro camera. As already mentioned, the MAVIC performs worse. As it can be seen from the parallel use of RAW (converted into TIF) and JPG image formats, the selection of image formats also influences the results from calibration. In Figure 8 the estimated position of principal point differs depending on the use of RAW (blue) or JPG (red) image format. Obviously it is not only the (physical) image format which changes, internally the camera adds other corrections, when converting into JPG. This is also illustrated in Figure 9, where the estimated lens distortion is shown for the Phantom 4 and Phantom 4pro camera. Again the results from using the RAW (converted to TIF) data are compared to the JPG images. It is quite obvious, that not only the image is converted to another data format, an additional a priori distortion correction is also applied, when changing formats their internal RAW to JPG. When this pre-corrected image is not fulfilling the model of central perspective, this will influence the quality of later calibrations. Thus, the use of uncompressed RAW image data is of advantage and should be recommended. Unfortunately most of the cameras need more time for the capturing of RAW image formats, which in a way limits the flights especially when high forward overlap is required and the flight speed cannot be decreased accordingly.

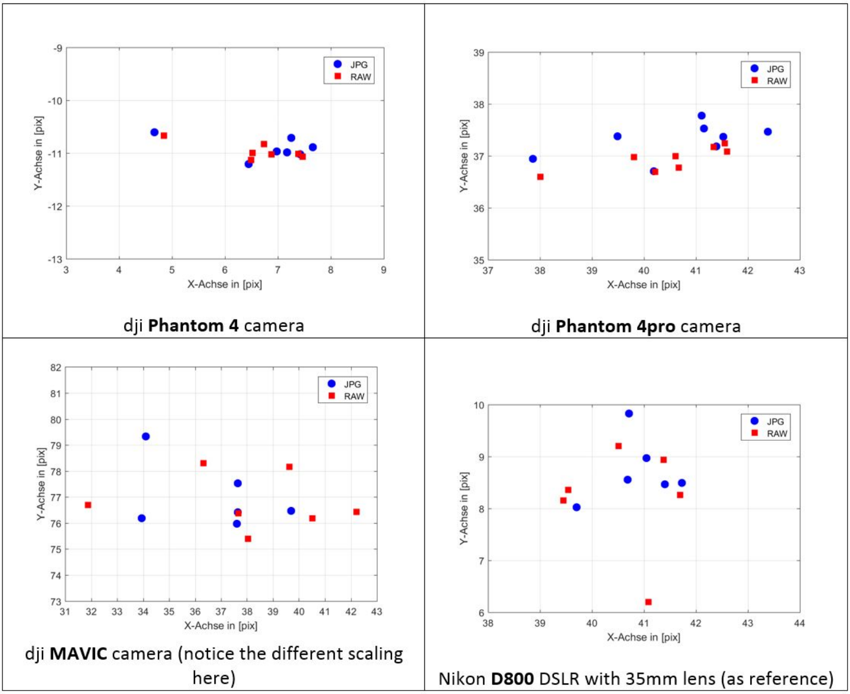

dji **Phantom 4** camera

dji **Phantom 4pro** camera

dji **MAVIC** camera (notice the different scaling here)

Nikon **D800** DSLR with 35mm lens (as reference)

Figure 8: Estimated principal point coordinates from several different calibration runs. Each point depicts one estimated principal point coordinate. The changes in stability are projected into the change of coordinates. Additionally the calibration differences using different image formats are visible.

The a priori lab calibration of (UAV-based) camera systems in general is not necessary, as later empirical flights have been shown, that on-site camera parameters quite differ from the geometrical lab calibration. The calibration of the camera with the methods of in-situ or self-calibration is sufficient but only works if the block has sufficiently good block geometry. As a rule, all blocks with overlapping parallel flight lines or 360° circular image blocks with a large image overlap (the latter can be realized through copter flights) should fulfill these prerequisites. Possibly it is helpful not to start in-situ calibration from zero values, but to use the previous calibration as an approximation. Especially the distortion of the camera system changes little.

If unconventional block geometry (for example, individual flight lines for corridor applications) is present, a best pre-calibrated camera must be requested. Ideally, this camera is calibrated in a close temporal and spatial context nearby the mission area (i.e. by using a test area) and these parameters are then adopted. For such applications, cameras with the

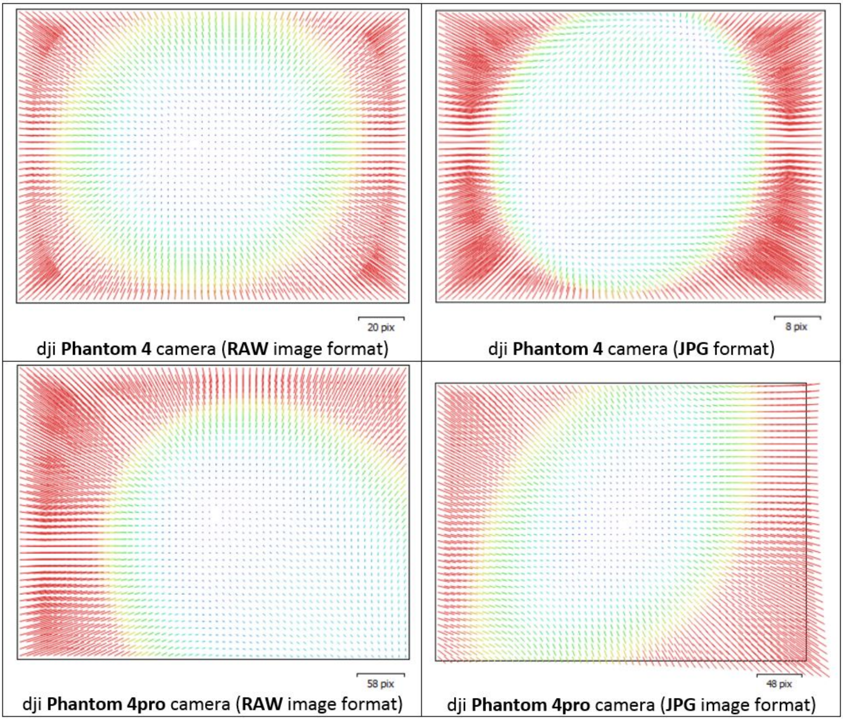

Figure 9: Estimated distortions using RAW and JPG image format. The distortions from JPG images are different to the RAW images. This clearly indicates, that a priori distortion correction is done in the camera when the JPG format is generated.

most stable camera geometry are preferred. In some circumstances, proprietary cameras, with fixed optics and fixed focus can be advantageous; alternatively specially developed (metric) cameras should be considered for these applications.

3D UAV flight planning for building reconstruction

Photogrammetric data capture of complex 3D objects using UAV imagery has become commonplace. Software tools based on algorithms like Structure-from-Motion and multi-view stereo image matching enable the fully automatic generation of densely meshed 3D point clouds. In contrast, the planning and execution of a suitable image network usually requires considerable effort of a human expert, since this steps directly influences the precision and completeness of the resulting point cloud. Planning of suitable camera stations can be rather complex, in particular for objects like buildings, bridges and monuments, which frequently feature strong depth variations to be acquired by high resolution images at a short distance. We developed an automatic flight mission-planning tool, which generates flight lines while aiming at camera configurations, which maintain a roughly constant object distance, provide sufficient image overlap and avoid unnecessary stations. Planning is based on a coarse Digital Surface Model and an approximate building outline. As a proof of concept, we use the tool within our research project MoVEQuaD, which aims at the reconstruction of building geometry at sub-centimeter accuracy. The project is funded by the Federal Ministry of Economic Affairs and Energy and is furthermore partnered by the Geodetic Institute of the University of Hannover and Geo-Office-GmbH.

A georeferenced 2.5D DSM, along with a 2D polygon describing the building contours, serve as main data input (Figure 10). We generate a volumetric occupancy map of the environment of the building, which classifies voxels of user-defined size into the classes: free space, object of interest, and obstacle (Figure 11). Optionally, an additional set of polygons may be used during map generation to define no-trespass areas. This option allows compensating for unreliably reconstructed areas in the DSM, e.g. poles, lanterns, vegetation, etc.

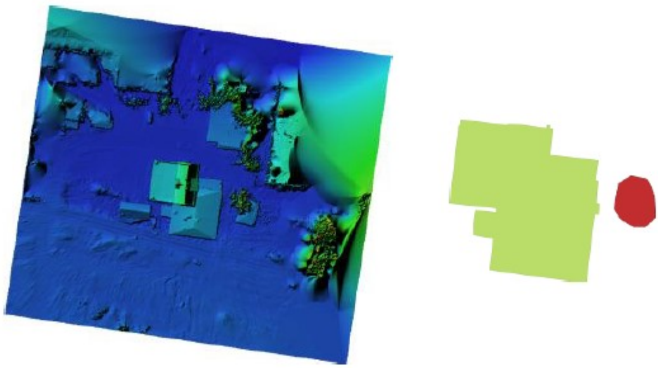

Figure 10: A DSM (left) and a polygon representing the building contour (green) is the main data input for mission planning. A single polygon (red) masks an imprecisely reconstructed tree close to the building.

Given a certain camera geometry, the camera should be positioned on the isosurface derived from „distance to object“ at value corresponding to the desired GSD. The viewing direction can be derived from the corresponding gradient. Intersection between the isosurfaces derived from „distance to occupied space“ and a safety distance removes unpassable parts. To ease these steps and the following ones, we perform these computations on z-layers of the volume, which correspond to fixed flight heights. The result is a set of trajectories for each flight height. Simple linking maneuvers connect these trajectories to a single mission (Figure 12).

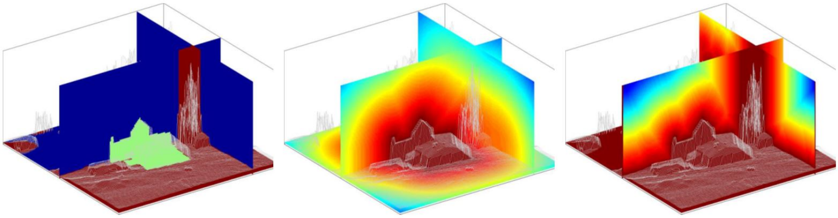

Figure 11: The volumetric map on the left segments space into the classes „object of interest“ (green), „obstacle“ (red) and „free space“ (blue). No-trespass areas create vertical obstacle areas. This map is combined with a three-dimensional scalar field, which holds distances to the object of interest (center). The result is a scalar field representing the distances to occupied space (right). It is used for obstacle avoidance during mission planning.

Figure 12: Top view of a flight plan. Green spheres with blue arrows indicate camera stations and corresponding camera alignment.

We developed a custom smartphone app to satisfy the particular needs of this project, which are primarily: assembling a flight mission, readable by the UAVs firmware, from given way-points and viewpoints of the flight plan, transferring it to an UAV and controlling the execution. Other solutions available on the market have been lacking certain features; many apps are designed solely for nadir flights.

The system was tested on-site with a low-cost quadrocopter (DJI Phantom 4 Pro). The resulting image distribution is homogeneous and covers the structures completely, while being well aligned towards the surfaces (Figure 14). Further, the number of captured images was reduced by more than 30% compared to a manual flight with time interval triggering. A comparison of time efficiency, however, is difficult, as the planned images were acquired on a rather windy day. Neglecting interruptions, the average time interval between images is 4.9s in comparison to 2.9s for the manual flight. Extrapolation to the image number results in ≈43min compared to ≈38min. De facto, a few interruptions are necessary to find good correction values for the trajectory, especially for the altitude, where the drone's self-localization deficiencies are most apparent. However, considering the larger area covered by the planned flights and the superior image distribution, we regard the test to be successful.

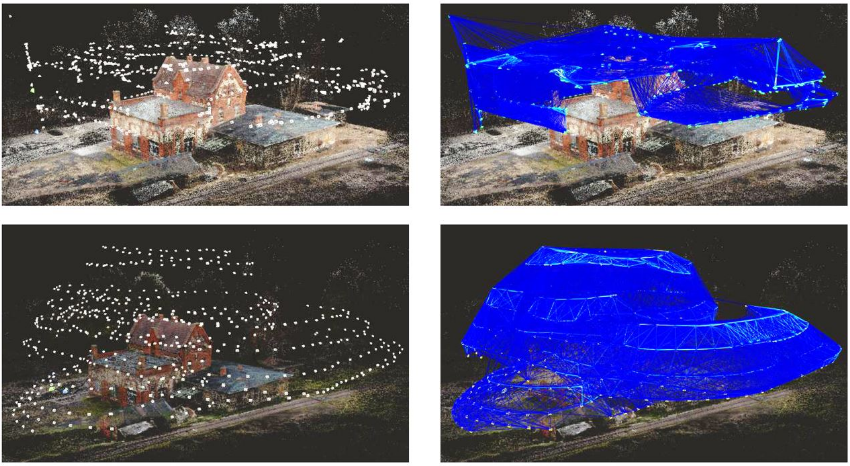

Figure 13: Comparison of image configurations resulting from a manually piloted attempt using time interval camera triggering (top) and from tests using our flight planning and assistance tools (bottom). In the former case, distances and viewing directions were not realised adequately. The distribution of camera stations (left) exhibits holes as well as clusters and results in suboptimal image connectivity (right). Using our approach, the results are significantly improved.

Close range photogrammetry for deformation measurement

Modern constructional steelwork is characterized by slim structures and production-optimized designs. Plates are often so slim, that they tend to bulge and bend under stress. The Institute for Construction and Design at the University of Stuttgart conducted large-scale experiments at the Materialprüfanstalt MPA in order to determine how accurate the theoretical description of these processes are. The examined steel beams are too large for a dense deformation tracking solely by local odometers etc. Therefore, we supported this project by implementing and operating a close range photogrammetric measurement setup and evaluation pipeline.

Figure 14: Meshed surface of the building, generated from UAV images. A precise, homogeneous and complete reconstruction was achieved with the well-distributed images of our flight planning and execution concept.

Four industrial IDS uEye provide the images. The cameras are mounted on individual tripods or installed into an aluminum profile frame with a fixed relative orientation, depending on the measured object. Baselines reach from 15cm to about 1.5m. Cables connect the cameras to a laptop directly via USB and indirectly via a microcontroller relay. We developed custom software for the operator to control the cameras. This configuration allowed reaching a deformation accuracy of ca. 0.1mm.

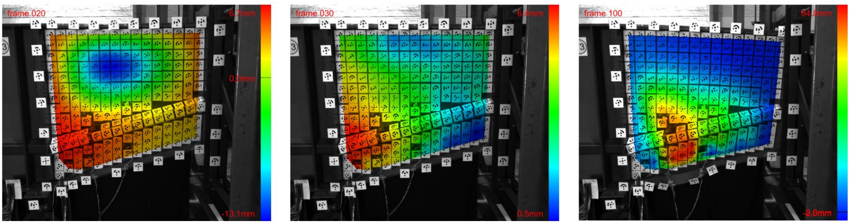

Frame 20 | Frame 30 | Frame 100

Figure 15: Frames showing the deformation of the outburst experiment.

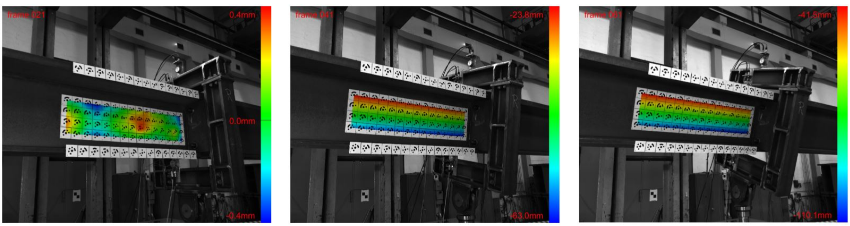

Frame 21 | Frame 41 | Frame 61

Figure 16: Frames showing the deformation of the twist and kink experiment.

Efficient engineer-geodetic monitoring of traffic structures

The lock Hessigheim is located at Neckar 143,01 km (see Figure 17) and built on unstable ground. Natural underground chambers arise due to eluviation of gypsum in the anhydrite layer. For this reason, the ground submerges continuously. The relative submergence of ground is about 1 mm/a up to 1 cm/a (relative to direct surroundings). The corresponding relative translatory movement is in the range of several mm/a. Absolute submergence is unknown. However, from a monitoring point of view relative movement is sufficient.

Figure 17: True Orthophoto (DOP) of the lock Hessigheim.

We monitor the lock in collaboration with the Bundesanstalt für Gewässerkunde (BfG) and the Amt für Neckarausbau Heidelberg (ANH).

The lock is monitored in a threefold manner:

- Engineer-geodetic monitoring (tachymeter, precise levelling, extensometer, alignment)
- Airborne monitoring (image matching, laserscanning)
- Satellite monitoring (persistent scatterer interferometry)

The objective of the project is to analyze different engineer-geodetic concepts for constructional questions. In particular, we analyze the potentials of area wide, permanent, high-frequency measurements for monitoring the lock.

Airborne monitoring (by image matching or laserscanning) and satellite monitoring (by persistent scatterer interferometry) are contactless measuring methods. Such remote sensing methods are capable to cover large areas in short time. In case of satellite sensors, temporal monitoring is possible. Depending on the repeat cycle of the satellite (usually between a few days up to weeks), time-series of imagery of high temporal density can be obtained.

Another aim of the project is to prove the efficiency for an area wide high-frequency monitoring regarding a high quality assurance. The subsequent aim is to apply the research findings/the concept to other traffic structures.

Engineer-geodetic monitoring

Engineer-geodetic monitoring is state-of-the art for highly accurate monitoring. However, the monitoring is only point based and very time-consuming. Furthermore, there are difficult geographic framework conditions at the lock that impede the monitoring. Common measurement tools are tachymeter, precise levelling, extensometer, and alignment.

Airborne monitoring (image matching, laserscanning)

The advantage of airborne imagery and airborne laserscanning is the generation of area wide, high-resolution point clouds. Furthermore, those points could be attached with semantic information. The standard multi-stereo image processing (matching, 3D reconstruction, DEM generation, generation of true orthophoto) has to be adapted to the challenging water surroundings. The same holds true for the standard laserscanning processing by the Laser Strip Adjustment. We seek to realize a ground sampling distance (GSD) of 3-5 mm and a minimal point density of 4 points per 10 x 10 cm. The combination of both methods generates a dense point cloud for every epoch. These point clouds can be used for generating difference models and, thus, for visualizing relative movements of objects.

Satellite monitoring (persistent scatterer interferometry)

We seek to detect movement of the lock with high accuracy and reliability based on Persistent Scatterer Interferometric Synthetic Aperture Radar (PSInSAR). We rely on TerraSAR-X and Sentinel 1 data. The main idea of Persistent Scatterer Interferometry is to detect pixels with a constant reflective behavior within a stack of radar images. Generally, these pixels correspond to rigid objects with smooth surfaces. Buildings are „natural" persistent scatterers in urban areas. In addition, we mount artificial persistent scatterers near the lock. These so-called corner reflectors (see Figure 18) work like retro reflectors.

First results

We achieved object point accuracy of 3-8 mm with our first monitoring flight in January 2018. Figure 19 shows the result of the matching. Figure 20 shows a first evaluation of PSInSAR.

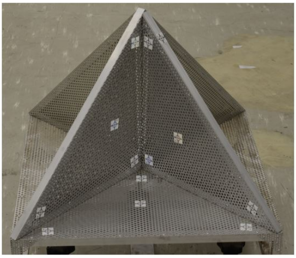

Figure 18: A corner reflector with targets for the determination of its phase center.

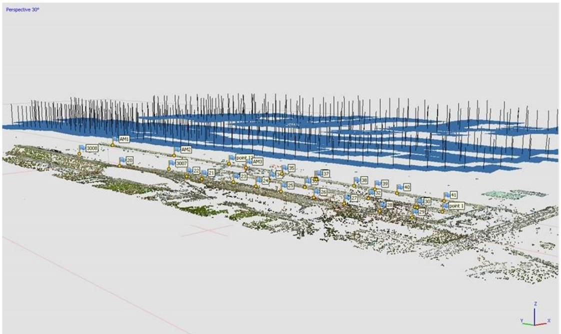

Figure 19: Result of the matching (thin point cloud and aligned images).

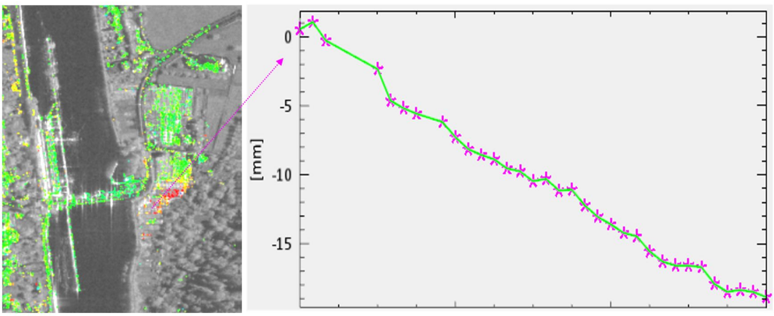

Figure 20: Left: Relative movement in the area near the lock Hessigheim (by PSInSAR). Red: high submergence, green: low submergence. Right: Accumulated displacement [mm] for one point (based on 33TerraSAR-X images. Period: 27th November 2014 - 28th December 2015).

Adaptive 4D PSI-based change detection

Previously, we proposed a PSI-based 4D change detection to detect disappearing and emerging PS points (3D) along with their occurrence dates (1D). Such change points are usually caused by anthropic events, e.g., building constructions in cities. This method first divides an entire SAR image stack into several subsets by a set of break dates. The PS points, which are selected based on their temporal coherences before or after a break date, are regarded as change candidates. Change points are then extracted from these candidates according to their change indices, which are modelled from their temporal coherences of divided image subsets. Finally, we check the evolution of the change indices for each change point to detect the break date that this change occurred. The experiment validated both feasibility and applicability of our method. However, two questions still remain. First, selection of temporal coherence threshold associates with a trade-off between quality and quantity of PS points. This selection is also crucial for the amount of change points in a more complex way. Second, heuristic selection of change index thresholds brings vulnerability and causes loss of change points. In this study, we adapt our approach to identify change points based on statistical characteristics of change indices rather than thresholding. The experiment validates this adaptive approach and shows increase of change points by at most 29% compared with the old version. In addition, we also explore and discuss the optimal selection of temporal coherence thresholds.

(a) (b)

Figure 21: Study area at the north of Berlin central station. (a) Mean TerraSAR-X image. (b) Aerial image (Google Earth) acquired on September 5, 2014. Yellow square, building construction.

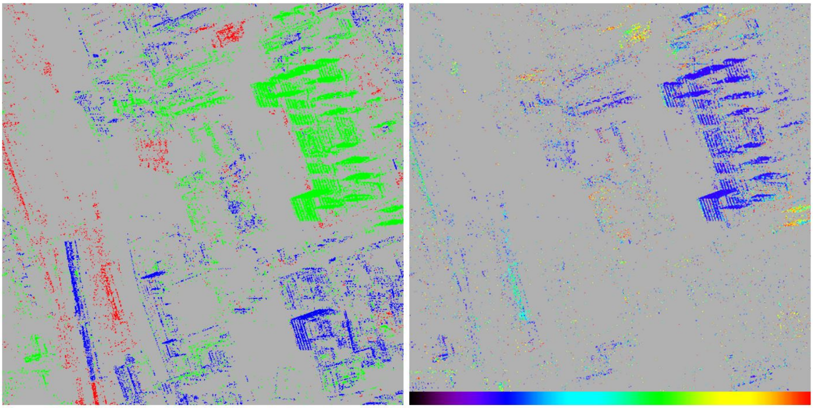

Figure 22: Spatiotemporal change detection result. (a) Steady, disappearing, and emerging structures represented by PS (blue), DBC (red), and EBC (green) points. (b) Occurrence dates: black to red, earliest to latest in 2013.

Modified epipolar resampling and orientation method for satellite imagery

Nowadays, high resolution satellite images have been commonly used for the point cloud and Digital Surface Model (DSM) generation or 3D reconstruction. Since we already have a completely workflow to process the satellite imagery, we focus more on the improvement of the pipeline.

New epipolar model

In order to get very dense point clouds, the modified Semi-Global Matching (tSGM) method is an efficient tool. Because the epipolar images will reduce the search range from 2D space to 1D space and largely decrease the processing time, epipolar resampling is required before the dense matching. As we know, the epipolar geometry of satellite pushbroom sensors only exists in small range areas, and the epipolar curve is more like a hyperbola line than a straight line. Many applications only carry out the epipolar resampling in small tiles. The present work aims at the epipolar resampling for the whole image without tiling. In our method, each epipolar curve is approximated by several segments. In order to get a proper epipolar segment length, we use the height range calculated from RPCs to define it. The sketch of the method is shown in Figure 23, and the main steps are:

- Select the points on the border as start points and calculate the epipolar line function
- Define the epipolar segment length and end point.
- Resample original image along the epipolar segment until it reach the end points
- Then choose the end point as the start point to derive new epipolar segments
- Repeat this procedure until the other border of the image is reached

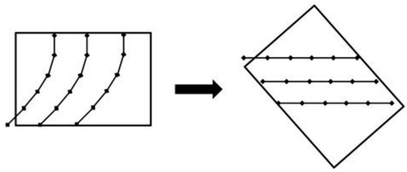

Figure 23: Epipolar curve approximation and resampling.

Epipolar curve approximation and resampling

All these steps are implemented with RPC projection trajectory method, and some evaluations have been done on QuickBird data that covers Melbourne. Twenty-five pairs of check points are selected to calculate the vertical parallaxes. The result is shown in Figure 24, all vertical parallaxes are smaller than one pixel and the root-mean-square (RMS) error is 0.499 pixels. This indicates that the piece-wise epipolar resampling method can reach sub-pixel level.

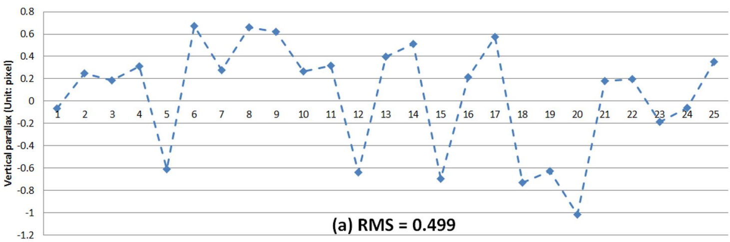

Figure 24: Vertical parallaxes of QuickBird Melbourne dataset.

Relative orientation without ground controls

From our experience, the Rational Polynomial Coefficients (RPCs) provided by the vendors are not always accurate enough. The corresponding points on matching image might not locate on the corresponding epipolar curve because of the lack of RPCs precision. Moreover, users might not have ground control information for bundle block adjustment. Therefore, relative orientation is an important pre-procedure to generate high quality epipolar geometry. Some researches use an error vector to compensate the error in matching image space, but only for small tiles.

The present work introduces a relative orientation method for entire satellite images without tiling. This method doesn't need ground control information, but only use the tie points and rough RPCs. The tie points are generated half-automatically with the software ENVI, and their accuracy is considered as sub-pixel level. The method measures the difference between corresponding points and corresponding epipolar curves on the matching image. Then we estimate an affine model as a global correction to compensate the location error for the whole image. Twenty-four check points are selected from the Pleiades imagery to verify the quality of this global compensated relative orientation. Before processing, the location error is as large as ca. 10 pixels. After the orientation, the location error is less than 1 pixel. The result is shown in Figure 25. According to the experiments, proposed relative orientation method can achieve sub-pixel accuracy and provide a good geometry for following epipolar resampling.

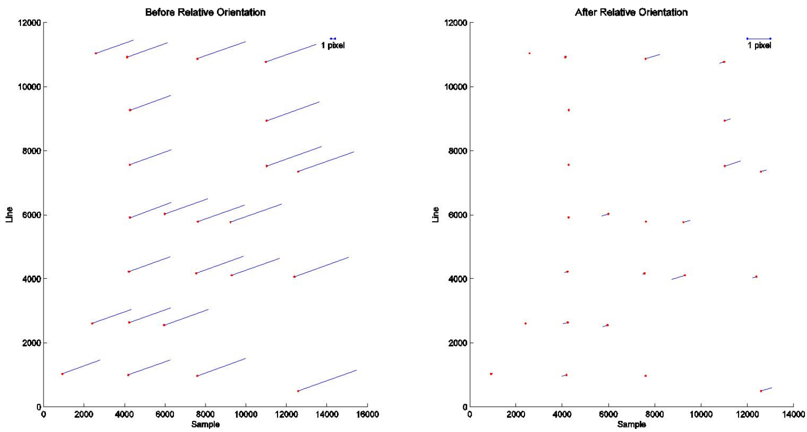

Figure 25: Location error of PleiadesTaibei dataset (the red points are the true corresponding points' location, blue lines are the distance between true location and the epipolar curve. The scale of the distance is shown in the right top of the figure).

Bathymetry by fusion of airborne laser scanning and multi-spectral aerial imagery

Knowledge about the bathymetry of water bodies is of high economic, social, and ecologic importance. Whereas charting bathymetry for navigational purposes is indispensable for ensuring safe shipping traffic, monitoring the quantity and quality of fresh water resources gains more and more importance, especially in the light of climate change. In the European context, three water related directives, namely the water framework directive (2000), the flood directive (2007), and the Fauna-Flora-Habitat directive (1992), request monitoring in a periodic cycle. Repeat acquisition of rivers and other inland water bodies is one of the essential tasks in fulfilling the above directives and requires efficient techniques for capturing bathymetry. The same applies to the coastal zone with applications in shore protection after storm events, monitoring of benthic habitats, etc.

Echo sounding is still the prime technique for capturing bathymetry. However, ship-borne sonar data acquisition is inefficient and even hazardous in shallow water areas. For surveying the bottom of the shallow riparian area, active and passive optical remote sensing techniques are employed. Three different approaches are in use: (i) Spectrally based depth estimation based on multi-spectral images, (ii) multi-media photogrammetry based on stereo images, and (iii) airborne laser bathymetry. Whereas the prior two are passive techniques using the reflections of solar illumination, the latter is an active method based on green laser radiation.

Exploiting the potential benefits of fusing concurrently acquired data from either data source (i.e. images and laser scans) is the topic of the German Research Foundation (DFG) project „Bathymetry by fusion of airborne laser scanning and multi-spectral aerial imagery“ that is work-in-progress at the Institute for Photogrammetry (project start: January 2017).

Modern airborne bathymetric sensors (e.g. Riegl VQ-880-G, Teledyne Optech CZMIL Nova, Leica/AHAB HawkEye III, etc.) incorporate laser scanners and multi-spectral cameras. This opens the floor for joint data processing of simultaneously acquired active and passive remote sensing data. Therefore, the following research topics are currently addressed at the IfP with the above-mentioned DFG project:

- Spectrally based depth estimation, through-water photogrammetry, and airborne laser bathymetry are used exclusively so far. It is expected that exploiting the complementary measurement techniques will result in more accurate, reliable, and complete Digital Terrain Models (DTM) of the submerged topography.
- Airborne Laser Bathymetry (ALB) is a monochromatic measurement technique operating in the green domain of the electro-magnetic spectrum. Especially for clear water, certain bands of multi-spectral or even hyper-spectral data may provide better water column penetration. This especially applies to the lower wavelength boundary of the visible spectrum (coastal blue-blue, λ=430-500nm).

- Depths derived from ALB constitute optimum reference data for calibrating models for spectrally based depth and/or substrate type estimation. This enables automated procedures for processing multi-spectral image data.

- The main advantage of ALB is that the derivation of depth relies on round-trip time measurement of a laser pulse and is, thus, independent from radiometric information (signal strength). Knowing the water depth reduces the unknowns for spectrally based techniques, which helps to distinguish substrate soil types, benthic habitats, etc. Fusion of passive image data and active laser scans should therefore improve the object classification (sand, gravel, rock, submerged vegetation, etc.).

- Existing state-of-the-art techniques like Conditional Random Fields can incorporate contextual information. Extending these techniques for the use with comprehensive active and passive remote sensing data as input should lead to better classification results.

- Whereas the laser footprint diameter fundamentally limits the spatial resolution of laser bathymetry, a much higher resolution in the range of the ground sampling distance of a single image pixel is achieved with Dense Image Matching. Embedding DIM in a multimedia-photogrammetry framework could potentially increase the DTM resolution of the littoral zone.

Following a literature research and an inspection of available laser and image data (coastal zone: German Baltic Sea; inland running waters: Pielach River, Austria), one of the main project activities in 2017 was planning and conducting a data acquisition campaign in the Stubai Alps (Tyrol, Austria). For this project, the IfP teamed up with the Unit of Hydraulic Engineering, University of Innsbruck (UIBK). The company Airborne Hydro Mapping (AHM) was commissioned to conduct a flight with a bathymetric laser scanner (Riegl VQ-880-G), a RGB camera (Hasselblad, 39 MP) and a separate Colour Infrared (CIR) camera for capturing two mountain lakes at the foothill of the Stubai glacier (Grünausee and Blaue Lacke). Both lakes are about 12m deep. In a first campaign in July 2017, the UIBK team measured the bathymetry of both lakes with a multi-beam echo sounder mounted on an inflatable dinghy. Within the same campaign, the IfP team (Gottfried Mandlburger, Ke Gong) measured twenty photogrammetric control points with Leica GNSS receivers. The IIGS (Andreas Kanzler, Annette Scheider) thankfully aided campaign with equipment and data processing support.

While the lakes featured very clear water in July (Secchi depth Grünausee: > 8m), the instable weather conditions prevented flight operation. Airborne data acquisition took place one month later on August 22. Whereas sunny weather and almost no wind provided excellent conditions for the flight, which was still challenging due to the extreme topography with surrounding peaks higher than 3.000m above sea level, several heavy thunderstorms in the beginning of August had a negative impact on the clarity of the lakes (Secchi depth Grünausee on August 22: 2.4m). As turbidity is the limiting factor for any optical measurement technique, only the near-shoreline area could be analysed so far. Figure 26 shows impressions and first results from the field campaigns in July and August.

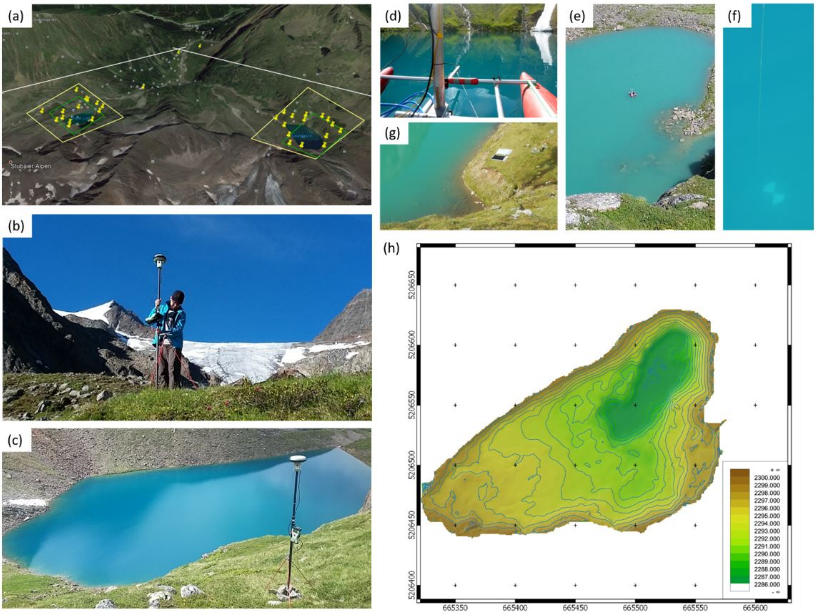

Figure 26: Study area Grünausee, Blaue Lacke, Stubai Alps, Tyrol, Austria; (a) flight planning; (b) Ke Gong (IfP) during GNSS surveying of a photogrammetric control point; (c) GNSS receiver in front of Blaue Lacke, July 2017; (d) multi-beam echo sounder mounted on inflatable dinghy; (e) sonar data acquisition of Blaue Lacke, July 2017; (f) Secchi depth measurement, Grünausee, July 2017 (> 8m); (g) radiometric control patches at the shore of Grünausee, August 2017; (h) submerged topography of Blaue Lacke derived from sonar data.

Apart from the Grünausee dataset, data from an existing flight in 2014 at the German Baltic sea, captured with a Leica/AHAB HawkEye III bathymetric laser scanner and an integrated RGBI camera (RCD30, 80 MPix) served as basis for a feasibility study on dense under-water matching. Figure 27 shows the first preliminary results, highlighting that the photogrammetric technique works well in shallow areas with calm water surface and high image texture, but fails in poorly textured areas with undulating water surface. A more sophisticated through-water dense image matching approach is currently work in progress, as are the remaining points from the above list of research topics.

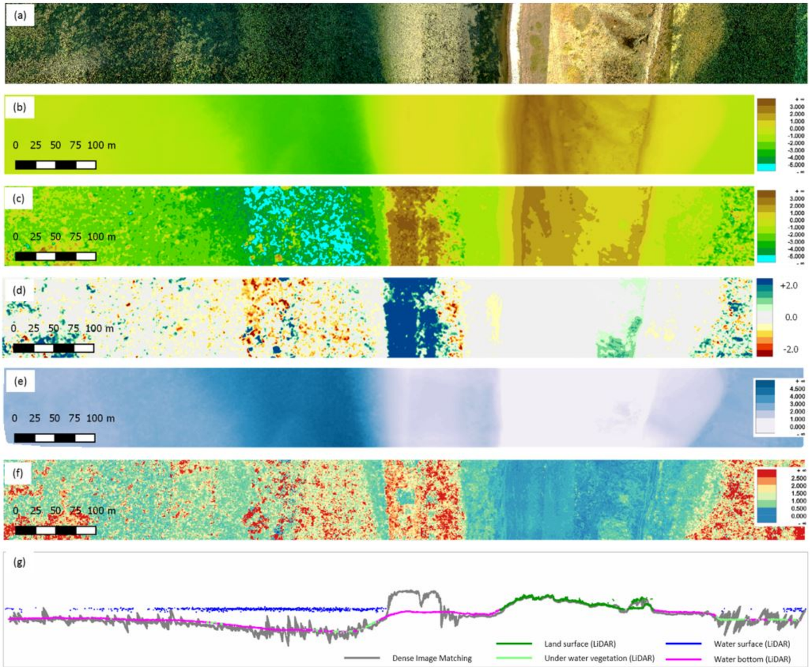

Figure 27: Study area Poel/German Baltic Sea; (a) colourised through-water DIM point cloud; (b) ALB DTM, colour coded elevation map; (c) DIM DTM, colour coded elevation map; (d) Colour coded DEM of Difference model (DIM minus LiDAR); (e) ALB derived water depth map; (f) RMSE of DIM point cloud (analysis unit: 25x25 cm^2); (g) DIM-ALB DTM profile comparison, location of section in the centre of the Figure 2a-f, complete East-West-transect, heights exaggerated (max. water depth: ca. 5m).

References 2017

Blaser, S., Nebiker, S., Cavegn, S.: System Design, Calibration and Performance Analysis of a Novel 360° Stereo Panoramic Mobile Mapping System. ISPRS Ann. Photogramm. Remote Sens. Spatial Inf. Sci., IV-1/W1, 207-213.

Cefalu, A., Haala, N., Fritsch, D.: Hierarchical Structure From Motion Combining Global Image Orientation and Structureless Bundle Adjustment. Int. Arch. Photogramm. Remote Sens. Spatial Inf. Sci., XLII-1/W1, 535-542.

Cefalu, A., Haala, N., Schmohl, S., Neumann, I., Genz, T.: A Mobile Multi-Sensor Platform for Building Reconstruction Integrating Terrestrial and Autonomous UAV-Based Close

Range Data Acquisition. Int. Arch. Photogramm. Remote Sens. Spatial Inf. Sci., XLII-2/W6, 63-70.

Cramer, M., Przybilla, H.J., Zurhorst, A.: UAV Cameras: Overview and Geometric Calibration Benchmark. Int. Arch. Photogramm. Remote Sens. Spatial Inf. Sci., XLII-2/W6, 85-92.

Cramer, M., Przybilla, H.J., Meißner, H., Stebner, K.: Kalibrierung und Qualitätsuntersuchungen UAV-basierter Kamerasysteme. Band 86/2017 DVW-SCHRIFTENREIHE, Wißner Verlag, 67-84.

Gong, K., Fritsch, D.: Relative Orientation and Modified Piecewise Epipolar Resampling for High Resolution Satellite Images. Int. Arch. Photogramm. Remote Sens. Spatial Inf. Sci., XLII-1-W1, 579-586.

Gu, H., Li, H., Yan, L., Liu, Z., Blaschke, T., Sörgel, U.: An Object-Based Semantic Classification Method for High Resolution Remote Sensing Imagery Using Ontology. Remote Sens. 2017, 9, 329.

Jhan, J. P., Rau, J. Y., Haala, N., Cramer, M.: Investigation of Parallax Issues for Multi-Lens Multispectral Camera Band Co-Registration. Int. Arch. Photogramm. Remote Sens. Spatial Inf. Sci., XLII-2/W6, 157-163.

Kenduiywo, B. K., Bargiel, D., Sörgel, U.: Higher Order Dynamic Conditional Random Fields Ensemble for Crop Type Classification in Radar Images. IEEE Transactions on Geoscience and Remote Sensing, 55(8), 4638-4654.

Mandlburger, G.: Interaction of Laser Pulse with the Water Surface - Theoretical Aspects and Experimental Results. Allgemeine Vermessungsnachrichten (AVN) 11-12/2017, 343-352.

Mandlburger, G., Pfeifer, N., Sörgel, U.: Water Surface Reconstruction in Airborne Laser Bathymetry from Redundant Bed Observations. ISPRS Ann. Photogramm. Remote Sens. Spatial Inf. Sci., IV-2/W4, 123-130.

Mandlburger, G., Wenzel, K., Spitzer, A., Haala, N., Glira, P., Pfeifer, N.: Improved Topographic Models via Concurrent Airborne Lidar and Dense Image Matching. ISPRS Ann. Photogramm. Remote Sens. Spatial Inf. Sci., IV-2/W4, 259-266.

Meißner, H., Cramer, M., Piltz, B.: Benchmarking the Optical Resolving Power of UAV Based Camera Systems. Int. Arch. Photogramm. Remote Sens. Spatial Inf. Sci., XLII-2/W6, 243-249.

Runceanu, L., Becker, S., Haala, N., Fritsch, D.: Indoor Point Cloud Segmentation for Automatic Object Interpretation. DGPF annual conference, Würzburg, Germany. Publikationen der DGPF, Band 26, 147-159.

Schack, L., Sörgel, U., Heipke, C.: Assigning Persistent Scatterers of Regular Multi-Story Buildings to Optical Oblique Images. PFG - Journal of Photogrammetry, Remote Sensing and Geoinformation Science, 85(1), 67-74.

Tutzauer, P., Haala, N.: Processing of Crawled Urban Imagery for Building Use Classification. Int. Arch. Photogramm. Remote Sens. Spatial Inf. Sci., XLII-1/W1, 143-149.

Wieser, M., Mandlburger, G., Hollaus, M., Otepka, J., Glira, P., Pfeifer, N. A Case Study of UAS Borne Laser Scanning for Measurement of Tree Stem Diameter. Remote Sensing. 2017, 9, 1154.

Yang, C.H., Sörgel, U.: Urban Monitoring by 4D Change Detection Using Multi-temporal SAR Images. DGPF annual conference, Würzburg, Germany. Publikationen der DGPF, Band 26, 2017, 233-244.

Yang, C.H., Sörgel, U.: Monitoring of Building Construction by 4D Change Detection Using Multi-temporal SAR Images. ISPRS Annals of The Photogrammetry, Remote Sensing and Spatial Information Sciences, IV-1/W1, 35-42.

Master Theses

Adam, J.R.: Markov Marked Point Process zur Klassifizierung von Gebäuden in 2.5D-Punktwolken. Supervisor: Becker, S.

Bashir, M.: Indoor Positioning for Warehouse Logistics. Supervisor: Walter, V.

Cruz Rangel, C.C.: Comparison and Implementation of Open Source Web Mapping Libraries as a Visualization Tool for the Conflict in Colombia. Supervisor: Walter, V.

Farmonov, E.: Implementation and Evaluation of a Crowd-based Approach for Georeferencing of Raster-Maps. Supervisor: Walter, V.

Graner, M.: Google Tango as an indoor mapping device. Supervisor: Runceanu, L.

Huang, X.: PCA-based change detection using multi-temporal SAR images. Supervisors: Yang, C.H., Sörgel, U.

Hurt, P.: Qualification and accuracy analysis of modern vehicle localization processes with the help of the entropy. Supervisors: Schuster, F. (Daimler AG), Haala, N.

Hüttl, P.: Structure from Motion for Oblique Aerial Imagery. Supervisors: Wenzel, K. (nFrames), Haala, N.

Iftikhar, M.A.: Spatially Aware Conversational Agent. Supervisor: Walter, V.

Ignat, P.: 3D indoor mapping using NavVis M3 Trolley data - an empirical study. Supervisors: Runceanu, L., Cramer, M., Fitz, D.

Jetter, M.: Überwachung von Veränderungen im urbanen Raum mittels SAR-Techniken - Fallbeispiel der Neuordnung des Bahnknotens Stuttgart. Supervisors: Yang, C.H., Sörgel, U.

Karam, S.: 3D-Building Reconstruction with Different Height Levels from Airborne LiDAR Data. Supervisor: Partovi, T. (DLR), Reinartz, P. (DLR).

Laupheimer, D.: Deep Learning for the Classification of Building Facades. Supervisors: Tutzauer, P., Haala, N.

Li, J.: Filtering terrestrial LiDAR point cloud in forest areas. Supervisors: Haala, N., Coughenour, C., Xie, H. (SGG, Wuhan University).

Li, P.: Evaluation and Improvement of a Dual-channel Method for Detection and Quantification of High-temperature Events Based on FireBIRD Data. Supervisor: Sörgel, U.

Liu, A.: Photogrammetric Data Collection and Processing - An Android App. Supervisor: Fritsch, D.

Lucaciu, F.: Estimating Pose and Dimensions of Parked Automobiles on Radar Occupancy Grids. Supervisor: Sörgel, U.

Mawas, K.: Close Range Photogrammetry, Computer Aided Design for Heritage Sites. Supervisors: Haala, N., Coughenour, C.

Moanta, A.M.: Camera-based Plough Control. Supervisors: Michalke, G. (Robert Bosch GmbH), Erz, M. (Robert Bosch GmbH), Haala, N.

Nhattiala, D.: Quality Analysis and Integration of Spatial Data. Supervisor: Walter, V.

Owda, A.N.: Digital Preservation of Calw Market Square - Im Zwinger by Means of Automated HDS and Photogrammetric Texture Mapping. Supervisors: Fritsch, D., Balsa-Barreiro, J.

Pang, H.: Application of Machine Learning Algorithms for the Automatic Recognition of Characters in Scanned Survey Plans. Supervisors: Heuchel, T. (Trimble/inpho), Tutzauer, P.

Pang, Y.: Time series change detection using SAR images: from pixel-based to object-based analysis. Supervisors: Yang, C.H., Sörgel, U.

Rajagopal, K.: Sharpness Optimization of a 3D Scanner Using Modulation Transfer Function. Supervisors: Döring, D. (FARO Scanner Production GmbH), Pfeiffer, R. (FARO Scanner Production GmbH), Haala, N.

Schmohl, S.: Study on Noise Robustness of 3D Shape Recognition with Convolutional Neural Networks. Supervisor: Sörgel, U.

Schwämmle, K.: 3D Reconstruction and texturing of the Copan Ruinas (Honduras) site using photogrammetry and LiDAR. Supervisor: Coughenour, C.

Shafaghi, Y.: A Geosocial Network for Refugees in Germany. Supervisor: Walter, V.

Song, Y.: Fusion of Range Data from Multi-View Stereo and LiDAR for Volumetric Surface Reconstruction. Supervisor: Cefalu, A.

Tang, M.: Calibration of automotive fish-eye cameras with misaligned camera components. Supervisors: Cramer, M., Singh, J. (Magna Electronics).

Thamarappilly, S.: Implementation of a GPS-based Android Game. Supervisor: Walter, V.

Vlachos, M.: Integration and Testing of Sequoia MS Camera with Various UAV Platforms. Supervisor: Cramer, M.

Zhang, X.: Fusion of Range Data from Multi-View Stereo and LiDAR for Volumetric Surface Reconstruction. Supervisors: Lombacher J. (Daimler AG), Broßeit, P. (Daimler AG), Haala, N.

Bachelor Theses

Budde, L.E.: Fusion von 3D-Punktwolken aus Stereo-Bildzuordnung und Laserscanning zur Verbesserung von digitaler Oberflächenmodellen. Supervisor: Mandlburger, G.

Clauß, D.: Integration von mehrfach erfassten Polygonen mit Hilfe eines Rasterbasierten Ansatzes. Supervisor: Walter, V.

Hirt, P.R.: Klassifizierung von 3D-Objekten in Gebäudeinnenräumen. Supervisor: Runceanu, L.

Joachim, L.: Potenzial von 3D-Punktwolken-basierter Unkrauterkennung in Mais. Supervisor: Reiser, D.

Lansche, L.: Untersuchung zur Qualität von DJI UAV-Kameras. Supervisor: Cramer, M.

Nied, F.: Band-zu-Band Registrierung UAV-gestützter MS-Kameras. Supervisor: Cramer, M.

Wiedemann, A.: Facade Detection in Urban Scenes using Semantic Image Segmentation. Supervisor: Tutzauer, P.

Activities in National and International Organizations

Cramer, M.:

Co-Chair ISPRS WG I/9: Integrated Sensor Orientation, Calibration, Navigation and Mapping

Englich, M.:

Webmaster ISPRS

Haala, N.:

Chair ISPRS WG II/2: Point Cloud Beneration
Vorsitz DGPF Arbeitskreis Sensorik und Plattformen

Sörgel, U.:

Vice President German Society for Photogrammetry, Remote Sensing and Geoinformation (DGPF)

Chair ISPRS WG III/3: SAR-Based Surface Generation and Deformation Monitoring

Walter, V.:

National Correspondent of the ISPRS Commission IV

Education - Lectures/Exercises/Training/Seminars

Bachelor „Geodäsie und Geoinformatik“

Geoinformatics I (Walter)	2/2/0/0
Geoinformatics II (Walter)	1/1/0/0
Image Processing (Haala)	2/1/0/0
Integrated Fieldworks (Haala, Keller, Kleusberg, Sneeuw)	0/0/4/0
Introduction into Geodesy and Geoinformatics (Cramer, Keller, Kleusberg, Sörgel, Sneeuw)	4/2/0/0
Photogrammetry (Cramer)	2/1/0/0
Remote Sensing (Sörgel)	2/1/0/0
Signal Processing (Sörgel)	2/1/0/0
Urban Planning (Dvorak)	2/0/0/0

Master Course „Geodäsie und Geoinformatik“

Aerotriangulation (Cramer)	1/1/0/0
Computational Geometry (Walter)	1/1/0/0
Computer Vision for Image-based Acquisition of Geodata (Haala)	1/1/0/0
Databases and Geographical Information Systems (Walter)	1/1/0/0
Digital Terrain Models (Haala)	1/1/0/0
Fundamentals in Urban Planning (Dvorak)	2/0/0/0
Georeferencing of photogrammetric Systems (Cramer)	1/1/0/0
Modelling and Visualisation (Haala)	1/1/0/0
Pattern Recognition and Image Understanding (Haala)	1/1/0/0
Remote Sensing (Sörgel)	1/1/0/0
Scientific Presentation Seminar (Haala)	0/0/0/2
Topology and Optimisation (Becker)	1/1/0/0
Web-based GIS (Walter)	1/1/0/0

Master Course GEOENGINE

Airborne Data Acquisition (Cramer)	2/1/0/0
Geoinformatics (Walter)	2/2/0/0
Signal Processing (Sörgel)	2/1/0/0
Image-based Data Collection (Haala, Cramer)	2/1/0/0
Integrated Fieldworks (Haala, Sneeuw, Keller, Kleusberg)	0/0/4/0
Remote Sensing (Sörgel)	2/1/0/0
Topology and Optimisation (Becker)	2/1/0/0

Master Course „Infrastructure Planning“

Introduction to GIS (Walter)	2/0/0/0

Master Course „Aerospace Engineering“

Image Processing (Haala)	2/1/0/0
Introduction into projective Geometry (Cramer)	2/0/0/0